11 October 2001

PHYSICS LETTERS B

ELSEVIER

Physics Letters B 518 (2001) 27–33

www.elsevier.com/locate/npe

Probing the ^{6}He halo structure with elastic and inelastic proton scattering

A. Lagoyannis[a,b], F. Auger[a], A. Musumarra[a,1], N. Alamanos[a], E.C. Pollacco[a], A. Pakou[b], Y. Blumenfeld[c], F. Braga[a], M. La Commara[d], A. Drouart[a], G. Fioni[a], A. Gillibert[a], E. Khan[c], V. Lapoux[a], W. Mittig[e], S. Ottini-Hustache[a], D. Pierroutsakou[d], M. Romoli[d], P. Roussel-Chomaz[e], M. Sandoli[d], D. Santonocito[c,1], J.A. Scarpaci[c], J.L. Sida[a], T. Suomijärvi[c]

[a] *DSM/DAPNIA CEA SACLAY, 91191 Gif-sur-Yvette, France*
[b] *Department of Physics, The University of Ioannina, 45110 Ioannina, Greece*
[c] *Institut de Physique Nucléaire, IN2P3-CNRS, F-91406, Orsay, France*
[d] *University of Napoli and INFN Sezione di Napoli, I-80125, Napoli, Italy*
[e] *GANIL, BP 5027, F-14021, Caen, France*

S. Karataglidis[f,g], K. Amos[h]

[f] *TRIUMF, 4004 Wesbrook Mall, Vancouver, British Columbia, V6T 2A3, Canada*
[g] *Theory Division, Los Alamos National Laboratory, Los Alamos, NM 87545, USA*
[h] *School of Physics, University of Melbourne, Melbourne, Victoria 3010, Australia*

Received 7 March 2001; received in revised form 12 June 2001; accepted 5 July 2001
Editor: V. Metag

Abstract

Proton elastic and inelastic scattering to the first excited state of ^{6}He have been measured over a wide angular range using a 40.9 *A* MeV ^{6}He beam. The data have been analyzed with a fully microscopic model of proton–nucleus scattering using ^{6}He wave functions generated from large space shell model calculations. The inelastic scattering data show a remarkable sensitivity to the halo structure of ^{6}He.

PACS: 25.60.-t; 25.40.Cm; 25.40.Ep; 24.10.Ht
Keywords: Unstable nuclei; Proton scattering; Optical model

It is well known that neutron rich weakly bound light nuclei have abnormally large radii [1]. This phenomenon is attributed to the valence neutrons which tunnel out of the core so that they have a large probability to be present at distances greater than the normal nuclear radius. Considerable experimental and theoretical efforts have been devoted to the understanding of the structure of these so-called halo nuclei [2,3]. However, due to the low intensities of the available

E-mail address: auger@hep.saclay.cea.fr, fauger@cea.fr (F. Auger).

[1] Present address: INFN-Laboratori Nazionali del Sud, Via S. Sofia 44, 95123 Catania, Italy.

0370-2693/01/$ – see front matter
PII: S0370-2693(01)00887-5

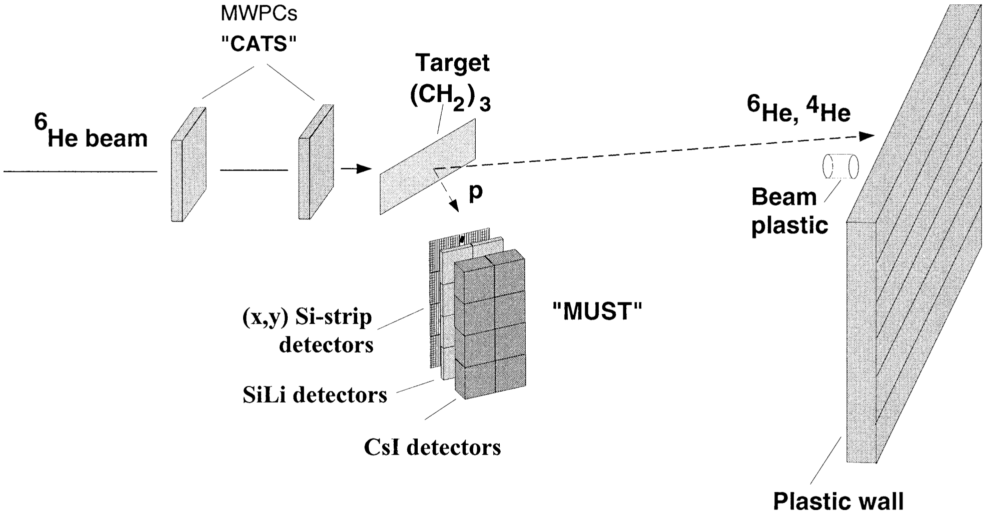

Fig. 1. The experimental setup. The trajectory of the beam was measured event by event by the CATS detectors. The recoiling protons were detected in the MUST array in coincidence with the ejectiles in the plastic wall.

exotic beams, it is only recently that inelastic scattering and transfer reactions on light particles, which are among the best tools to probe deeply the structure of nuclei, could be undertaken under good conditions. Experimentally, the Borromean ^{6}He nucleus is an eminently suitable candidate for this kind of study since the first excited state is the 2^+ state at 1.87 MeV [4]. It has been investigated through the measurement of interaction, dissociation and elastic scattering cross sections [5]. However, apart from elastic scattering, those reactions involve breakup of the ^{6}He into its constituents ($^4\mathrm{He} + n + n$) and all the results indicate that there is no sensitivity to the microscopic structure of the projectile [6].

To study the microscopic structure of ^{6}He we measured elastic and inelastic scattering of ^{6}He from protons by making use of a new large acceptance detector array MUST [7]. In this Letter, extended angular distributions are presented along with a fully microscopic analysis using wave functions generated from large space shell model calculations allowing all the nucleons of ^{6}He to be active (no core shell model).

The experiment was performed at the GANIL facility with a 40.9 A MeV ^{6}He radioactive ion beam produced by fragmentation of a primary 75 A MeV ^{13}C beam on a 8.45 mm thick C target located in the SISSI device [8]. The secondary beam was purified with a 0.9 mm thick Al degrader situated between the dipoles of the α-spectrometer. The beam intensity on the polypropylene $(CH_2)_3$ reaction target was 10^5 particles per second with a 2% total contamination of ^{8}Li and ^{9}Be. As the beam spot on the target covered 1 cm^2 with a maximum angular divergence of 1°, two X and Y position sensitive detectors, CATS [9], were placed at 155 cm and 27 cm in front of the target as illustrated in Fig. 1. These detectors provided the impact point (X, Y) and the incident angle (Θ) on the target event by event with a FWHM resolution of 0.55 mm (X), 0.7 mm (Y) and 0.1° (Θ).

The recoiling protons were detected in MUST [7], an array of 8 three-stage telescopes 6 cm × 6 cm each. The first stages consist in double-sided Si-strip detectors (300 µm). They were placed at 15 cm from the target and covered the angular range between 46° and 90° in the laboratory frame. At this distance, the 1 mm wide strips result in an angular resolution of 0.4° in both X and Y directions. Protons of less than 6 MeV were stopped in these detectors and were identified down to 0.5 MeV by measurement of energy versus time of flight (E-TOF). The start of the TOF measurement was given by the passage of the incident particle in one CATS tracking detector and the overall time resolution was 1.2 ns. Protons in the energy range of 6 to 25 MeV were stopped in the second SiLi stage

(3 mm) of the telescopes while those in the energy range from 25 to 70 MeV were stopped in the third CsI stage (15 mm). They were identified by the ΔE–E method.

The ejectile was detected in coincidence with the recoiling proton to suppress the protons emitted from excited nuclei produced in central collisions of ^{6}He on the carbon contained in the target. The coincidence allowed also suppression of protons coming from reactions induced by the beam contaminants on the target. The ejectile was detected in a plastic wall, situated at 75 cm behind the target and made up of 6 horizontal bars of BC408, 8×50 cm^2 and 3 cm thick. Each bar was read out by a photo-multiplier at each end. The large angular coverage of the wall was imposed by the in flight decay of ^{6}He ($^6\mathrm{He} \rightarrow \alpha + 2n$) that occurs for excitation energies higher than the $2n$ separation energy of 0.9 MeV [4]. Identification and counting of the beam particles were achieved in a plastic scintillator with a diameter of 2.8 cm and centered at zero degrees.

To measure angular distributions down to 10° in the center of mass (85° in the laboratory) where the energy of the recoiling protons decreases down to 0.5 MeV, a 1.48 mg/cm^2 thick polypropylene target (density, 0.896 g/cm^3) was used. Good statistics at larger angles was obtained by using a 8.25 mg/cm^2 thick target. Protons were selected with contours on the E-TOF and ΔE–E planes of MUST. The excitation energy spectrum of ^{6}He calculated from energy and angle of the protons detected between 46° and 65° in the laboratory (without requiring a coincidence with the plastic wall) is shown in Fig. 2(a). The excitation energy resolution is equal to 800 keV and no other excited state appears above the well known 2^+ at 1.8 MeV. Elastic, respectively, inelastic events were extracted from inclusive events by requiring that a ^{6}He, respectively, an alpha particle be detected in the plastic wall in coincidence with the proton. The selection in the plastic wall was done by doing contours on the E-TOF matrix. Fig. 2(b) shows the excitation energy spectrum for the inelastic events associated to protons detected between 60° and 70°. Despite the coincidence with the ejectile it remains a contamination from elastic scattering due to the insufficient energy resolution of the plastic wall. Events corresponding to the excitation of the 2^+ state were extracted from inelastic events by taking a window between 0.8 and 2.3 MeV. The high energy side of

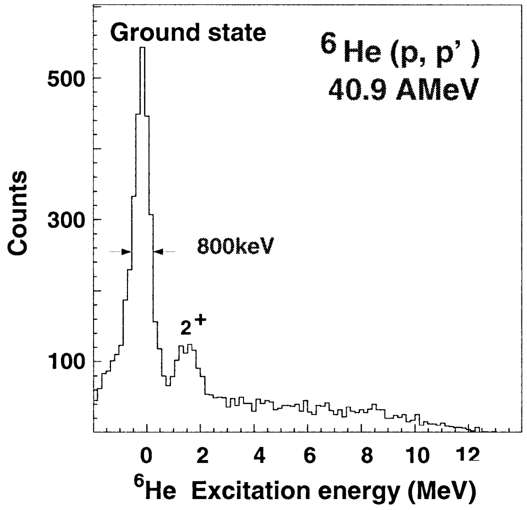

(a)

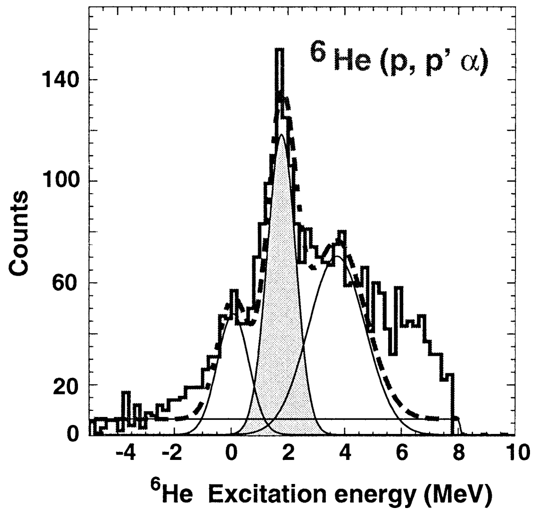

(b)

Fig. 2. (a) ^{6}He excitation energy spectrum extracted from protons detected between 46° and 65° in the laboratory, (b) ^{6}He excitation energy spectrum extracted from protons detected between 60° and 70° in the laboratory in coincidence with an alpha particle. Four components have been considered to estimate the background under the 2^+ peak (see text).

the 2^+ peak is contaminated by low lying excitations in the continuum and by the fragmentation processes. Part of the constant background is due to reactions with the ^{12}C of the target. The coincidence between the recoiling proton and the ejectile suppresses most of this contamination but it remains a small constant background. In order to estimate the background under the 2^+ peak, for each bin of 2° in the laboratory, the spectrum was fitted with four components as shown in Fig. 2(b). They are (i) a small constant background corresponding to the background observed at the left of the elastic peak, (ii) and (iii) two Gaussians for the elastic and inelastic peaks having the same width as the ^{6}He elastic peak, and (iv) a third Gaussian beginning above the $2n$ separation energy (0.9 MeV) to simulate the excitations in the continuum. To estimate the uncertainty on the background subtraction, the fit was made also with a linear component rather than the third Gaussian and/or a maximum constant background at the level of counts measured at -2 MeV excitation energy. With these different assumptions the background under the 2^+ peak varied between 13% and 17% for the spectrum shown in Fig. 2. It represents between 10% and 30% of the peak depending on the angle. The uncertainty on this value stands at $\pm 5\%$ for all angles. Elastic and 2^+ state contributions were extracted for each 1° bin in the laboratory frame and normalized with the acceptance of the detection system, the target thickness ($\pm 5\%$ uncertainty) and the number of incident ^{6}He ($\pm 3\%$ uncertainty).

Angular distributions in the center of mass are presented in Fig. 3. The error bars given for elastic scattering are purely statistical whereas the error bars quoted for the inelastic scattering include, in addition, the error due to the background subtraction.

Calculations for the elastic proton scattering data were made using a fully microscopic model of the optical potential [10]. In this model, the potential is obtained in coordinate space by folding a complex energy- and density-dependent effective nucleon–nucleon (NN) interaction with the one-body density matrix elements (OBDME) and single particle bound states of the target generated by shell model calculations. As the approach accounts for the exchange terms in the scattering process the resulting complex optical potential is non-local. We refer to it as the g folding potential. This model has been applied successfully to calculate elastic and inelastic scattering of protons from many stable and unstable nuclei ranging from ^{3}He to ^{238}U at different energies between 65 MeV and 300 MeV [11–14]. The effective interaction and the structure details were all preset and no *a posteriori* adjustment or simplifying approximation was made to the folded optical potentials. Hence the observables obtained are predictions.

Calculations of the transition amplitudes for the inelastic scattering have been done within the distorted wave approximation (DWA). The same effective NN interaction and shell model calculations used to make the g folding optical potential have been, respectively, used for the transition operator and the transition OBDME. For the stable nuclei whose spectroscopy is well defined from the measurement of inelastic electron scattering form factor, the inelastic scattering has been shown to be very sensitive, more than elastic scattering, to the details of the effective interaction [11]. Conversely, when the effective interaction was well established, the analysis of inelastic data turned out to be a very sensitive test of the model structure used for the nucleus [11,12]. As for elastic scattering the calculations were parameter free.

To apply these models to 40 MeV proton scattering, the effective NN interaction had to be determined. As for the higher energies, it has been parametrized as a sum of central, two-body spin–orbit and tensor components, each of them being a set of Yukawa functions of various ranges. This specific form is dictated by the structure chosen in the program DWBA98 [15] which has been used for the analysis of both the elastic and inelastic scattering data. The complex, energy- and density-dependent strength and the range of each Yukawa function were obtained by accurately mapping the on- and half-on-shell g matrices which are solutions of the Brueckner–Bethe–Goldstone equations of the Bonn-B [16] realistic NN interaction. The validity of the 40 MeV effective interaction has been verified by calculations of cross sections and analyzing powers of proton elastic scattering for different stable nuclei [17].

With the effective NN interaction set, it remained only to define the structure of ^{6}He. A view that this nucleus should resemble an α particle with two extraneous neutrons has fostered a semi-microscopic cluster model treatment of the system [18]. On the other hand, large space (no-core) shell model calculations [19,20] and quantum Monte Carlo calculations [21] which are fully microscopic have been done. The Navrátil and Barrett [19] large space shell model calculations are suited to our scattering analyses. They allowed the 6 nucleons to be active and their

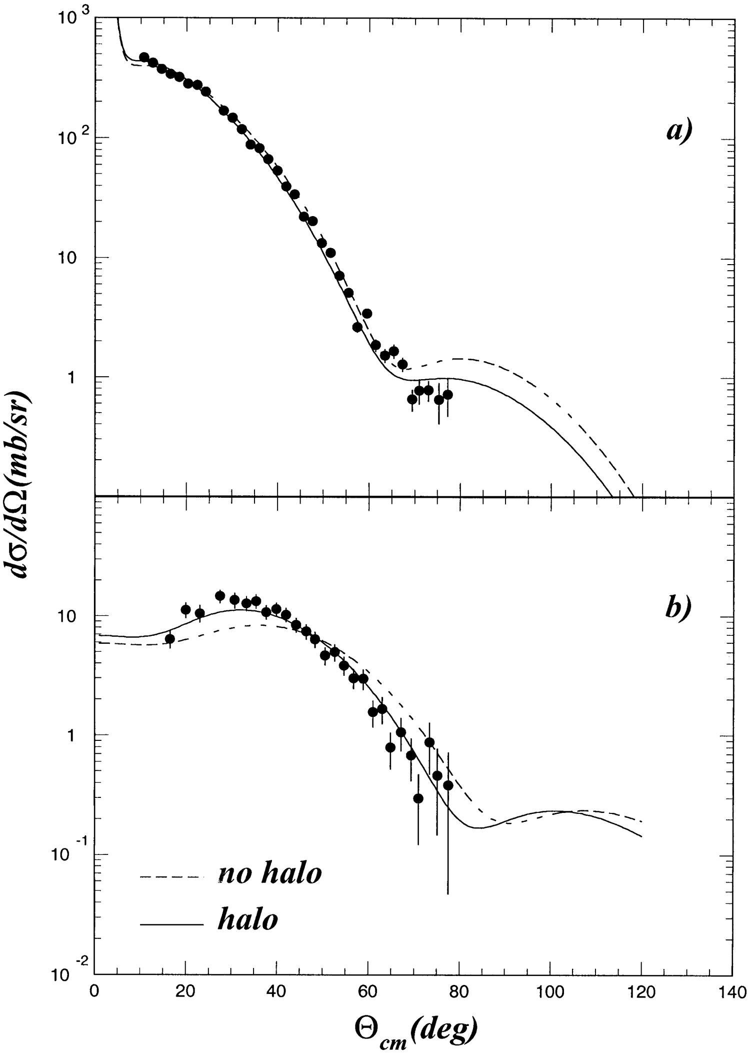

Fig. 3. Differential cross sections for the (a) elastic and (b) inelastic scattering to the of 2^+ state at 1.87 MeV of ^{6}He from hydrogen at 40.9 A MeV. The present data (circles) are compared to the results of the calculations assuming no halo (dashed line) and halo (solid line) conditions.

shell model interaction was specified as NN G matrix elements [22] generated from the realistic CD-Bonn NN interaction. We used their complete $6\hbar\omega$ wave functions to specify the relevant ground state and $0^+ \to 2^+$ transition OBDME for ^{6}He. To investigate the sensitivity of the analyses on the size of the model space we have also used wave functions from a complete $4\hbar\omega$ shell model [20]. In the latter model, the wave functions obtained are $|0_1^+; 1\rangle = 77.95\%|0\hbar\omega\rangle + 11.01\%|2\hbar\omega\rangle + 11.04\%|4\hbar\omega\rangle$ and $|2_1^+; 1\rangle = 68.47\%|0\hbar\omega\rangle + 19.35\%|2\hbar\omega\rangle + 12.18\% \times |4\hbar\omega\rangle$, indicating that most of the transition occurs in the $0p$-shell. However, in both models the binding energy of the last neutron is larger than the experimental separation energy 1.87 MeV [4]. That would indicate that the size of the model spaces used is still too small to give the correct asymptotic behavior of the neutron density.

The p–^{6}He g folding optical potential made with the shell model prescribed Harmonic Oscillator (HO) functions is almost phase shift equivalent to that obtained using Wood–Saxon (WS) functions which allow to fit electron scattering for form factor of ^{6}Li [12]. This led us to use these WS functions but in order to specify the neutron halo in ^{6}He we changed the bound state WS potential so that the $0p$-shell binding energy became 2 MeV which is close to the single neutron separation energy. Also the binding energies of the higher orbits were all set to 0.5 MeV as more exact (smaller) values will not influence noticeably results of the scattering. The optical potential obtained using these adjusted WS single particle wave functions leads to the cross section hereafter designated as *halo*. This is consistent with the use by Millener et al. [23] of WS functions in specifying halo densities when using shell model wave functions. Hence, the use of the HO single particle wave functions given by either shell model leads to the cross section that we designated as *no halo*. The *no halo* and *halo* neutron and proton density distributions have been published in [20]; they correspond to r.m.s. matter radii of 2.3 and 2.58 fm, respectively. The *halo* matter r.m.s. radius is consistent with those obtained from few-body model analyses of elastic scattering and reaction cross sections [20].

Note that the labelling of *halo* and *no halo* is used merely to distinguish between the two sets of calculations. The *no halo* case may correspond to the situation in which the nucleus exhibits a skin; any shell model calculation for nuclei with $N > Z$ will automatically generate such a skin in the density (see, for example, Ref. [20]). The halo itself has an additional feature: to conserve particle number, the nucleon density must be depleted at the center of the nucleus. This manifests itself in a decrease in the elastic scattering cross section at large angles [20].

The elastic scattering data are compared in Fig. 3(a) to the *halo* (solid line) and *no halo* (dashed line) calculations. The two calculations are very similar up to 60° and notably differ at larger angles. The agreement of the calculations with the data is very good up to 60°. The few data beyond these angles are better reproduced by the *halo* description but it is clear that data at larger momentum transfers are required to use elastic scattering as a probe of the halo structure of ^{6}He.

The very good agreement obtained with the elastic scattering data is essential since it validates the g folding optical potential used to define the distorted waves in the DWA analysis of the inelastic scattering leading to the 2^+; $T = 1$ state. *Halo* (solid line) and *no halo* (dashed line) calculated cross sections for the 2^+ state are presented in Fig. 3(b). Contrary to the elastic scattering, the sensitivity to the halo is important over the entire angular domain. The data are very well reproduced by the *halo* calculation. This conclusion is strengthened by the fact that the results for both elastic and inelastic scattering obtained by using $4\hbar\omega$ [20] rather than $6\hbar\omega$ model space wave functions and also by using the Paris Potential [24] rather than the Bonn-B interaction are very similar. The validity of the models used to predict the present data is corroborated by the very good agreement for the reaction cross section obtained between the *halo* result of the $4\hbar\omega$ model (353 mb and 406 mb for the *no-halo* and *halo* cases, respectively) and the experimental value (409 ± 22 mb [25]).

In conclusion, we have presented data for the elastic and inelastic (2^+) scattering of ^{6}He from hydrogen at $40.9A$ MeV over a large angular domain (10° to 80°). An excellent prediction of both elastic and inelastic data has been made using a fully microscopic, complex, non-local optical potential based on large basis shell-model calculations of ^{6}He with the incorporation of a neutron halo. On the other hand, we have shown that the 2^+ state scattering data are not reproduced by using the unaltered shell model wave functions which over-predict the binding energy of the valence neutrons and thus do not allow the halo to be formed. The sensitivity of the inelastic scattering data to the structure of ^{6}He and the success of the coordinate space scattering theories, based upon effective NN interactions used successfully in analyses of proton scattering from stable nuclei, open large perspectives for the study of the microscopic structure of exotic systems.

References

[1] I. Tanihata, Nucl. Phys. A 478 (1988) 795c.
[2] P.G. Hansen et al., Annu. Rev. Nucl. Part. Sci. 45 (1995) 591.
[3] B. Jonson, K. Riisager, Philos. Trans. R. Soc. (London) A 356 (1998) 2063.
[4] F. Ajzenberg-Selove, Nucl. Phys. A 490 (1988) 1.
[5] I. Tanihata et al., Phys. Lett. B 160 (1985) 380;
I. Tanihata et al., Phys. Lett. B 289 (1992) 261;
J.S. Al-Khalili et al., Phys. Lett. B 378 (1996) 45;

G.D. Alkhasov et al., Phys. Rev. Lett. 78 (1997) 2313;
A.A. Korsheninnikov et al., Nucl. Phys. A 617 (1997) 45;
M.D. Cortina-Gill et al., Nucl. Phys. A 641 (1998) 263;
T. Aumann et al., Phys. Rev. C 59 (1999) 1252.
[6] D. Aleksandrov et al., Nucl. Phys. A 633 (1998) 234.
[7] Y. Blumenfeld et al., Nucl. Instrum. Methods A 421 (1999) 471.
[8] W. Mittig, Nucl. Phys. News 1 (1990) 30.
[9] S. Ottini et al., Nucl. Instrum. Methods A 431 (1999) 476.
[10] P.J. Dortmans, K. Amos, Phys. Rev. C 49 (1994) 1309.
[11] S. Karataglidis et al., Phys. Rev. C 52 (1995) 861;
S. Karataglidis et al., Phys. Rev. C 52 (1995) 3224;
S. Karataglidis et al., Phys. Rev. C 53 (1996) 838;
P.J. Dortmans et al., Phys. Rev. C 57 (1998) 2433;
P.J. Dortmans et al., Phys. Rev. C 58 (1998) 2249.
[12] S. Karataglidis et al., Phys. Rev. C 55 (1997) 2826.
[13] P.J. Dortmans et al., J. Phys. G 23 (1997) 183;
P.J. Dortmans et al., Phys. Rev. C 55 (1997) 2723.
[14] S. Karataglidis et al., Phys. Rev. Lett. 79 (1997) 1447.
[15] J. Raynal, Computer code DWBA98, NEA 1209/05, 1999.
[16] R. Machleidt et al., Phys. Rep. 149 (1987) 1.
[17] P.K. Deb et al., Phys. Rev. C 62 (2000) 037601.
[18] K. Arai et al., Phys. Rev. C 59 (1999) 1432, and references cited therein.
[19] P. Navrátil, B.R. Barrett, Phys. Rev. C 54 (1996) 2986;
P. Navrátil, B.R. Barrett, Phys. Rev. C 57 (1998) 3119.
[20] S. Karataglidis et al., Phys. Rev. C 61 (2000) 024319.
[21] B.S. Pudliner et al., Phys. Rev. C 56 (1997) 1720.
[22] D.C. Zheng et al., Phys. Rev. C 52 (1995) 2488.
[23] D.J. Millener et al., Phys. Rev. C 28 (1983) 497.
[24] M. Lacombe et al., Phys. Rev. C 21 (1980) 861.
[25] A. de Vismes et al., Phys. Lett. B 505 (2001) 15.